https://doi.org/10.48048/tis.2024.7534

Improving Pb(II) Removal via Ascorbic Acid-Enhanced Red Mud Adsorption: Kinetics and Isotherm Analysis

Berlian Sitorus[1,*], Theo Yoyo[1], Septami Setiawati[2] and Syahrul Khairi[3]

[1]Department of Chemistry, Universitas Tanjungpura, Pontianak, Indonesia
[2]Department of Mining Engineering, Universitas Tanjungpura, Pontianak, Indonesia
[3]Department of Chemical Engineering, Universitas Tanjungpura, Pontianak, Indonesia

([*]Corresponding author's e-mail: berlian.sitorus@chemistry.untan.ac.id)

Received: 25 September 2023, Revised: 30 November 2023, Accepted: 7 December 2023, Published: 10 April 2024

Abstract

This study explored the efficacy of red mud, an aluminum production by-product, as an adsorbent for Pb(II) ion removal from contaminated water and assessed the adsorption isothermal model and kinetics. Red mud, characterized by its richness in oxide minerals with reactive surfaces, has potential for heavy metal adsorption, but its capacity for larger ions like Pb(II) is limited. This research aimed to enhance red mud's adsorption properties through modification with ascorbic acid. The modification process involved heating a mixture of red mud and ascorbic acid to its boiling point, followed by the formation of adsorbent beads using red mud and Na-alginate mixture dropped into a 2 % $CaCl_2$ solution at −2 °C. The beads were tested over varying durations ranging from 30 to 210 min. The results indicated that ascorbic acid modification led to the transformation of minerals in red mud, improving its pore diameter, pore volume, and specific surface area of the adsorbent. The modified and unmodified red mud adhered to both Langmuir and Freundlich isotherms, with R^2 values converging to one, and displayed pseudo-second-order kinetics. Notably, the introduction of ascorbic acid augments the adsorption efficacy of red mud for Pb(II) ions from 84.8 % to a compelling 99.3 %. This underscores the augmented capability of ascorbic acid-modified red mud, highlighting its prospective applicability as a potent adsorbent in the remediation of heavy metal-contaminated water.

Keywords: Adsorption effectiveness, Adsorption kinetics, Adsorption isothermal model, Ascorbic acid modification, Langmuir and Freundlich isotherm, Pb(II) ion removal, Pseudo-second-order kinetics, Red mud

Introduction

The environmental accumulation of red mud takes up considerable land area and poses risks such as soil alkalinization and groundwater and air contamination [1]. Despite its widespread availability, the application of red mud is limited, with only 2 - 3 % being used in cement and ceramic manufacturing [2]. A potentially effective method of utilizing red mud is converting it into an adsorbent, given its richness in alumina (Al_2O_3) and silica (SiO_2) [3], which allows for a large surface area. This makes red mud a viable adsorbent for heavy metals like Pb(II) ions in aqueous solutions [4].

Pb(II) ions are hazardous waste in aquatic environments, primarily from industrial, mining, and metal processing activities. This leads to enduring water pollution and presents significant global challenges [5,6]. Prolonged exposure to Pb ions is associated with severe health issues, including damage to the liver and kidneys, encephalopathy, and potential genetic harm [7]. Numerous studies have aimed to develop efficient strategies for Pb ion removal, with adsorption standing out as a favored and effective approach. Due to its high oxide mineral content, red mud holds potential as an adsorbent for Pb(II) ions due to its ability to form negatively charged structures that bind with positively charged metal ions [8]. However, a challenge arises from its relatively low adsorption capacity for large-radius Pb metal ions[9].

Efforts to activate red mud, such as using hydrochloric acid, have been effective for smaller radius metal ions like Cr(II), but less so for larger ions like Pb(II) [10]. Therefore, enhancing the adsorption effectiveness and capacity by modifying red mud's physicochemical properties is crucial. Researchers in [11] successfully increased adsorption effectiveness by 83.4 % by modifying red mud with hydrazine sulfate. A promising approach involves the use of ascorbic acid, an eco-friendly reducer capable of converting 97 - 98 % of red mud into a magnetic adsorbent, thereby increasing adsorption affinity for heavy metal ions, such as Cu(II) in aqueous solution [12,13].

The imperative drove this research to augment the potential of red mud for adsorbing Pb(II) ions through modification with ascorbic acid. This study seeks to harness the potential of red mud for adsorbing Pb(II) ions by incorporating ascorbic acid. The central objective is to bolster the efficiency of red mud as an adsorbent using this modification. Ascorbic acid, an eco-friendly reducing agent, can transform up to 97 - 98 % of red mud into a magnetic adsorbent. Furthermore, it promotes the -OH and carboxylate functional groups on the adsorbent's surface, enhancing its adsorption capacity for heavy metal ions [12,13]. The pressing nature of this work arises from the necessity to mitigate environmental concerns, both by minimizing the extensive land area designated for red mud storage and by developing low-cost adsorbent raw materials for heavy metals, especially Pb(II), to efficiently reduce water pollution. Therefore, the central objective of this study is to transform red mud into a product of economic value rather than allowing it to persist as waste.

Materials and methods

Materials

In this research, the red mud was sourced from PT.ICA, West Kalimantan. Other materials in this study were: L(+)-Ascorbic Acid for analysis, $C_6H_8O_6$ 99.7 % (Merck, Germany), filter paper Whatman 42 (GE Healthcare, USA), distilled water, calcium chloride, Sodium alginate (HiMedia Laboratories, India), and Lead(II) nitrate ($Pb(NO_3)_2$ and $CaCl_2$ from (Emsure-Merck). The instruments included a centrifuge (Oregon), Buchner funnel, beaker glass, sonicator, 100-mesh sieve, hot plate stirrer, standard laboratory glassware, oven, and shaker.

Methods

Preparation of Modified and Unmodified Red Mud

The preparatory method adopted in this study draws upon several references, specifically [13,14]. Initially, the raw red mud was washed and dried at 105 °C. Post-drying, the red mud was pulverized and sieved using a 100-mesh test sieve. Subsequently, the sieved red mud underwent another washing and drying cycle at 105 °C for 4 h. The dried red mud was then further processed and sieved through a 200-mesh sieve to secure red mud particles of 75 microns, subsequently labeled as unmodified red mud (U-RM). For the modification process, 7 g of unmodified red mud was combined with 7 g of ascorbic acid, previously dissolved in 50 mL of distilled water, and brought to a boil at 190 °C. Then the mixture was filtered with Whatman 42 filter paper to collect the residue after being cooled to room temperature, washed, and dried at 105 °C for an hour. The red mud, now treated with ascorbic acid, was stored in a dark, airtight container and labeled as modified red mud (M-RM). Immobilization of Red Mud was performed as the following. Both prepared types of red mud, modified RM and unmodified RM, were immobilized using Ca-alginate. One gram of Na-Alginate was mixed in 50 mL of deionized water until dissolved and then stirred at a rotation of 1000 rpm at 85 °C until homogeneous. Subsequently, with continuous stirring, 0.5 g each of modified RM and unmodified RM were introduced to a solution containing sodium alginate. The resultant mixture was cooled and dripped into a 2 % $CaCl_2$ solution, pre-cooled to −2 °C, and left to stand for 24 h to form beads. The beads were rinsed thrice using purified water, subsequently subjected to drying at 80 °C, and stored in an airtight bottle. These beads were then employed as adsorbents for Pb metal ions.

Adsorbent evaluation and analysis

Both the modified RM and unmodified RM adsorbents were characterized using FTIR and GSA. Atomic Absorption Spectrophotometer (AAS) were used in this research. The FTIR spectra were recorded using a Prestige-21 Spectrophotometer, Shimadzu, FTIR Spectrophotometer, collected over the range of 4000 - 400 cm^{-1}. The purpose of FTIR characterization was to identify the functional groups present in the adsorbents. Meanwhile, Surface Area Analyzer (BET) characterization assessed physical attributes such as surface area, pore volume, and diameter using Gas Sorption Analyzer (GSA) Quantachrome Novatouch LX-4. The testing principle employed by this tool involves quantifying the gas adsorption on the surface or within the pores of a solid material under conditions of constant pressure and temperature, with nitrogen gas as the selected medium.

Batch adsorption experiment

Adsorption experiments were performed in sealed polypropylene bottles at ambient temperature. For each test, 0.3 g of ascorbic acid-modified (M-RM) beads were immersed in 150 mL of a 20 mg/L Pb(II) solution with a pH of 6.

This procedure was mirrored for the U-RM. In each instance, the adsorbent and Pb(II) solution were agitated on a shaker at 350 rpm for specific time intervals: 30, 60, 90, 120, 150, 180, and 210 min. Subsequently, the residual Pb(II) was isolated with a 0.45 µm filter and quantified via AAS.

The adsorption capacity of the adsorbent and the percentage removal of metal ions were then calculated using Eqs. (1) and (2) [13]:

$$q = \frac{(C_0 - C_t)}{m} V \quad (1)$$

$$\%R = \frac{(C_0 - C_t)}{C_0} \times 100 \quad (2)$$

where: C_0 (mg/L) and C_t (mg/L) represent the initial and equilibrium concentration of Pb(II), respectively; q (mg.g^{-1}) represents the mass of the Pb(II) or Mn (II) adsorbed by each gram of the modified red mud. The volume of the adsorbate solution in L is denoted by V (L), while m (g) represents the mass of the absorbent.

Further adsorption experiments were conducted varying the adsorbate concentrations. An amount of 0.3 g of adsorbent was introduced to Pb(II) solutions with concentrations of 20, 40, 80, 160, and 320 ppm. The mixtures were agitated at 350 rpm, based on the optimal duration identified earlier. Following this, the residual Pb(II) was again extracted with a 0.45 µm filter. All Pb(II) concentration measurement for absorption data was taken by using a graphite furnace, AAnalyst 700 Atomic Absorption Spectrometer, Perkin-Elmer. The adsorption experiments were conducted in triplicate to assess the reproducibility of the results.

Both adsorption equilibrium and kinetics data were acquired from batch experiments. Adsorption equilibrium studies were conducted by employing various adsorbate concentrations. A total of 0.3 g of adsorbent was introduced into Pb(II) solutions with respective concentrations of 20, 40, 80, 160, and 320 ppm. The mixture was then agitated using a shaker at an optimum speed of 350 rpm for the predetermined duration, as in the previous treatments. Following agitation, the residual Pb(II) (referred to as aliquot/Pb(II)) was extracted through a 0.45 µm filter and subsequently analyzed using the AAS instrument. The adsorption isotherms were determined using the Langmuir and Freundlich models. All the experiments were carried out at room temperature (28 ± 2 °C).

Results and discussion

FTIR analysis

Before and after modification with ascorbic acid, the red mud samples were characterized using FTIR, as depicted in **Figure 1**. The FTIR analysis results reveal broadened peaks at wavelengths 3449 cm^{-1} for unmodified RM and 3478 cm^{-1} for modified RM, respectively. The emergence of these broadened peaks in the 2500 - 3750 cm^{-1} range can be attributed to the O-H group of water, gibbsite, and alginate molecules [15,16]. Peaks are also evident in the 1700 - 3000 cm^{-1} range, indicative of the silanol OH group [15].

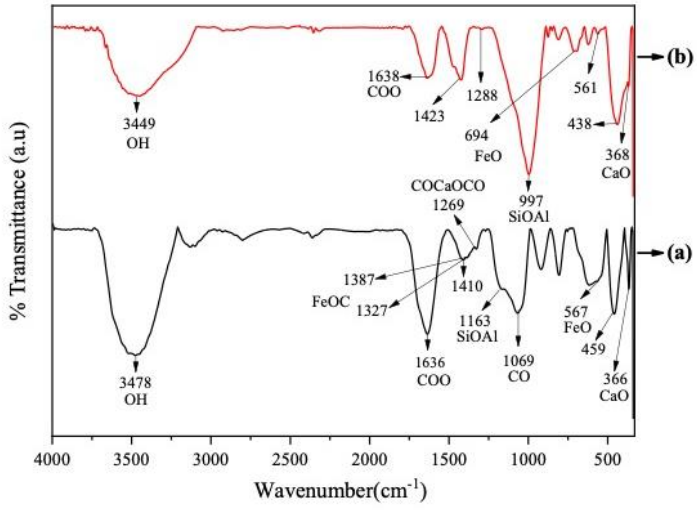

Figure 1 FTIR spectra of (a) Modified Red Mud (M-RM), and (b) Unmodified Red Mud (U-RM).

The FTIR analysis for the unmodified RM sample revealed a spectral peak within the 997 - 1008 cm^{-1} range, indicative of the presence of Si-O-Al groups in the sample. A noticeable shift in the spectrum peaks of the RM samples was observed upon modification with ascorbic acid. This shift, or the emergence of a new peak in the 1075 - 1190 cm^{-1} range, can be attributed to the Si-O-Al found in morimotoite and cancrinite minerals, as highlighted by Chukanov and Vigasina [16]. Morimotoite and cancrinite minerals are formed by reducing andradite and hematite minerals by ascorbic acid [12].

Examining the fingerprint region of the ascorbic acid-modified red mud through FTIR analysis revealed the existence of Fe-O groups, specifically at the 567 cm^{-1} spectrum peak, deriving from the Fe_3O_4 mineral. This particular peak is associated with the stretching of the Fe-O group in the formed magnetite mineral (Fe_3O_4). This Fe-O group is also discernible in the U-RM sample, exhibiting a band at the absorption peak of 561 cm^{-1}, correlating with the Fe-O bending vibration in the Fe_2O_3 mineral. Further observations of the Fe-O bending vibrations of Fe_2O_3 are evident at the 694 - 711 cm^{-1} spectrum peak. Interestingly, this peak is absent in the ascorbic acid-modified red mud sample, signifying the lack of Fe-O bending vibrations in the modified sample. This observation aligns with the understanding that ascorbic acid reduces the hematite mineral in red mud to magnetite mineral [17]. Moreover, the strain of Fe-O (tetrahedral) is also detected in the 438 cm^{-1} region, shifting to 459 cm^{-1} in the modified adsorbent, representing the strain of Fe-O (both tetrahedral and octahedral) as documented by Pham *et al.* [18].

Crosslinking of Ca-alginate was evidenced in both M-RM and U-RM samples, specifically at the spectral peaks of 1269 and 1288 cm^{-1}. These peaks are attributed to the vibrations of the carboxyl bonds in alginate interacting with Ca^{2+} ions, as depicted in **Figure 1**. Additionally, the spectral peaks at 1635 and 1638 cm^{-1}, corresponding to M-RM and U-RM, respectively, represent the symmetric carboxylic group (COO) strain, while the peaks at 14010 cm^{-1} (M-RM) and within the range of 1423 - 1472 cm^{-1} (U-RM) indicate the asymmetric carboxylic group (COO) strain [19]. Vibrations associated with Ca-O are also present, appearing at wave numbers 366 cm^{-1} for M-RM and 368 cm^{-1} for U-RM adsorbent.

The primary alcohol C-O group in ascorbic acid is notably prominent, exhibiting strong intensity at the spectral peak of 1069 cm^{-1}; this is characteristic of the typical absorption band of the primary alcohol C-O group, which ranges between 1000 - 1075 cm^{-1} [20]. Notably, this C-O group is solely observed in the ascorbic acid-modified red mud sample.

Moreover, the stretching vibration of the C=O group of cyclic esters (lactones, COO-C- in ascorbic acid and alginate) is discernible at the spectral peaks of 14,010 cm^{-1} (M-RM) and 1423 cm^{-1} (U-RM). The strain present in the Fe-O=C bond of red mud interacting with alginate is evident in both M-RM and U-RM, with the appearance at wave numbers 1269 and 1288 cm^{-1}, respectively.

Brunauer-Emmett-Teller (BET) surface area analysis

The adsorbent, presented as beads, was characterized to determine the adsorbent's surface area, pore diameter, and pore volume. The results of the characterization are displayed in **Table 1**.

Tabel 1 BET analysis results.

Adsorbent	S_T / Specific surface area (m^2/g)	S / Surface area (m^2/g)	V/Pore Volume (cm^3/g)	d/Pore Diameter (nm)
M-RM	177.4	14.5	0.04	0.86
U-RM	146	11.3	0.03	0.75

M-RM: Modified Red Mud
U-RM: Unmodified Red Mud

As depicted in **Table 1**, the BET analysis results reveal that the adsorbent exhibits a pore diameter range of 0.75 - 0.86 nm. This range categorizes the adsorbent as microporous since, adsorbents with a pore diameter of less than 2 nm fall under the microporous type [5]. Modifying red mud with ascorbic acid enhances specific surface area, pore volume, and pore diameter. These enhancements in the M-RM sample can be attributed to alterations in the chemical components of red mud, thereby leading to changes in the physical properties of the adsorbent.

Surface area, pore volume, and pore diameter are essential for a solid material to possess adsorptive capabilities. These factors significantly influence the increase in adsorption capacity and the effectiveness of physical adsorbents, albeit having minimal impact on chemical adsorption. The unmodified red mud adsorbent exhibited an increase in pore diameter after being utilized for the adsorption of Pb(II) metal ions. This increase is associated with diffusion occurring in the adsorbent pore following interaction with the adsorbate solution [9]. The pore volume of the adsorbent before adsorption ranged from 0.027 to 0.38

cm^3/g. This pore volume is sufficient for Pb(II) ions to access the RM adsorbent, which has a hydrated radius of approximately 0.401 nm [21].

Adsorption test

The adsorption test was conducted by preparing a 20 ppm Pb(II) solution. This was achieved by weighing 0.3 g of $Pb(NO_3)_2$ salt and dissolving it in 1 L of solution. Subsequently, the pH of the resulting solution was adjusted to 6, identified as the optimum pH for the adsorbent to function effectively [13]. Once the pH of the adsorbate reached 6, the adsorbent was introduced to each Pb(II) solution and agitated using a shaker. Adsorption tests were performed with time variations of 30, 60, 90, 120, 150, 180, and 210 min. The percentage of adsorption effectiveness is represented in **Table 2**.

Table 2 Adsorption effectiveness percentage of the modified and unmodified adsorbents for Pb(II).

Adsorbent	Effectiveness of adsorption over various time (%)						
	30 min	**60 min**	**90 min**	**120 min**	**150 min**	**180 min**	**210 min**
M-RM	70.1	80.7	87.3	90	94.6	96.7	99.3
U-RM	43.5	64.7	72.5	78.5	79.3	82.7	84.8

The Pb(II) adsorption test, utilizing the modified red mud adsorbent, immobilized with calcium alginate, exhibited an optimum time of 210 min and achieved an adsorption percentage of 99.3 %, as depicted in **Table 2**. These results substantiate that the red mud adsorbent, modified with ascorbic acid, effectively adsorbs Pb(II) metal ions, as also explained by Babu *et al.* [11].

Modification through ascorbic acid has been shown to enhance the effectiveness of red mud as an adsorbent. The unmodified red mud adsorbent could only adsorb 84.8 % of Pb(II) metal from a 20 ppm Pb(II) concentration. Post adsorption, the concentration of residual Pb(II) ions was 3.04 ppm using U-RM adsorbent; in contrast, with the M-RM adsorbent, the residual Pb(II) ion concentration was reduced to 0.15 ppm. As an example of regulation, according to the Regulation of the Indonesian Minister of Environment and Forestry, No. 5, Year 2022, the permissible limit of Pb(II) in waters surrounding industrial areas is 1 ppm. Furthermore, the Government Regulation of the Republic of Indonesia, No. 22, Year 2021, stipulates that the maximum Pb(II) concentration in waters allocated for agriculture is 0.5 ppm. The ascorbic acid-modified adsorbent demonstrates promising results, showcasing its potential to mitigate metal pollution in water bodies.

Adsorption isotherm model

The adsorption process or mechanism in place is determined by the Langmuir and Freundlich adsorption isotherm models. The Langmuir adsorption isotherm is formulated as depicted in Eq. (3a) and subsequently simplified to a linear equation, as shown in Eq. (3b).

$$Q_e = \frac{K_L Q_m C_e}{1+K_L C_e} \quad (3a)$$

$$\frac{C_e}{Q_e} = \frac{1}{K_L Q_m} + \frac{1}{Q_m} C_e \quad (3b)$$

where: Q_e ($mg.g^{-1}$) is the Pb(II) amount adsorbed onto adsorbent at equilibrium; Q_m represents Langmuir maximum adsorption capacity (in $mg.g^{-1}$); K_L is the Langmuir sorption constant, which is related to the adsorption energy ($L.mg^{-1}$) and Ce ($mg.L^{-1}$) is the equilibrium concentration of Pb(II) in aqueous solution.

The Langmuir isotherm graph is generated from the linear Eq. (3b), plotting Ce/Qe versus Ce. The concentration of the solution after adsorption (Ce) was obtained from the results of measuring the adsorbate after adsorption with AAS. The Langmuir isotherm describes the adsorption process that occurs chemically by forming a monolayer layer.

On the other hand, Freundlich adsorption isotherm is formulated based on Eq. (4a) which is then reduced to a linear equation as in Eq. (4b).

$$Q_e = K_f C_e^{1/n} \quad (4a)$$

$$\log Q_e = \log K_f + \frac{1}{n} C_e \quad (4b)$$

where: K_f is Freundlich capacity factor constant ($L.g^{-1}$), and (1/n) represents isotherm linearity parameter constant.

Analogous to the approach used for the Langmuir isotherm, the Freundlich isotherm graph is constructed using linear Eq. (4b) by plotting log Qe versus Ce. The concentration of the solution after adsorption, Ce, is determined by measuring the adsorbate post-adsorption using AAS. The Freundlich isotherm illustrates the adsorption process as a physical one, resulting in the formation of a multilayer.
The adsorption isotherm graphs are depicted in **Figure 2** for the unmodified red mud and in **Figure 3** for the modified red mud adsorbent. The graphs resulting from these linear equations can be employed to determine the Langmuir parameters (KL and Qm) as well as the Freundlich parameters (K_f and n).

Based on **Figure 2**, the adsorption isotherm graph of ascorbic acid-modified red mud, it is evident that the R^2 for the Freundlich adsorption isotherm is 0.8993, and the Langmuir adsorption isotherm has an R^2 of 0.9638. **Figure 3**, depicting the adsorption isotherm graph of unmodified red mud adsorbent, reveals R^2 of 0.9463 and 0.9949 for the Freundlich and Langmuir isotherms, respectively. Based on the R^2 for both samples, it can be concluded that the adsorption isotherm models for both are Langmuir and Freundlich. The Langmuir adsorption isotherm is associated with a chemisorption process that occurs through the formation of a monolayer or single layer on the adsorbent's surface, while the Freundlich isotherm is employed to determine the physical adsorption process that occurs on the surface of the adsorbent's heterogeneous active groups [22,23].

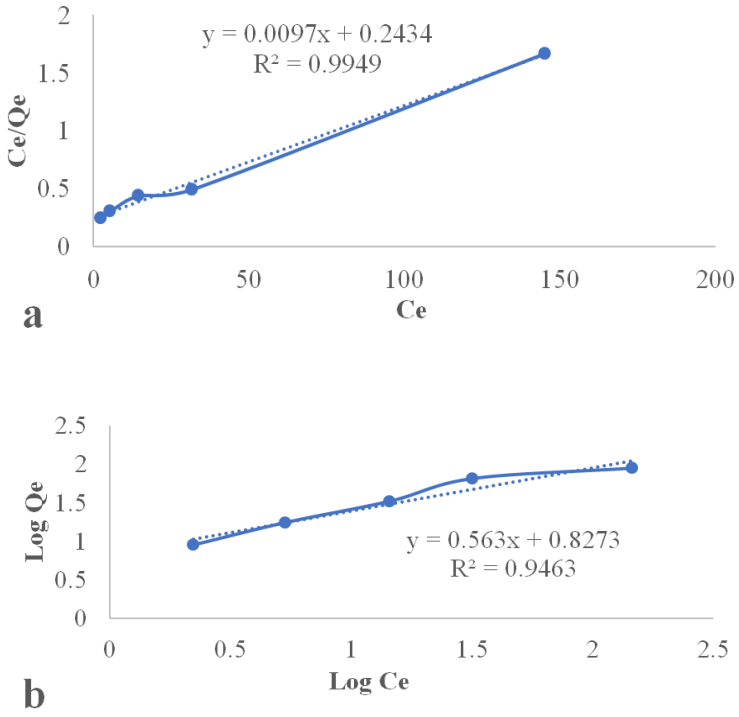

Figure 2 The adsorption isotherms of the unmodified red mud (U-RM) adsorbent: (a) Langmuir isotherm, and (b) Freundlich isotherm.

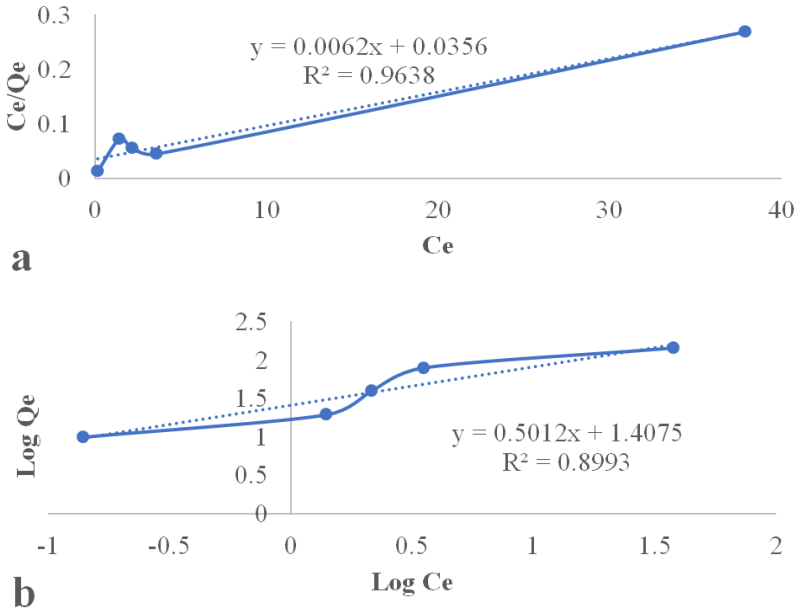

Figure 3 The adsorption isotherms of the modified red mud (M-RM) adsorbent: (a)Langmuir isotherm, and (b)Freundlich isotherm.

After plotting the data from adsorption experiments for both modified and unmodified red mud adsorbent, based on Eqs. (3b) and (4b), the Langmuir parameters (K_L and Q_m), as well as the Freundlich parameters (K_f and n), can be calculated, and these results are provided in **Table 3**.

Table 3 Langmuir parameters and Freundlich parameters (K_f and n) Adsorption Isotherm for M-RM and U-RM adsorbent.

Adsorbent	Langmuir			Freundlich		
	K_L (L/mg)	Qm (mg/g)	R^2	K_f (mg/g)(L/g)$^{1/n}$	n	R^2
M-RM	0.17	161.3	0.96	25.56	1.99	0.90
U-RM	0.04	103.1	0.99	6.72	1.78	0.95

The adsorption capacity of the modified adsorbent experienced an increase due to the formation of numerous carboxylate and OH active groups, resulting from the reaction of ascorbic acid with red mud. These active groups are categorized as hard bases, thus they bind more readily with Pb^{2+} ions, which are intermediate acids [24]. These minerals are oxide minerals enriched with electron-rich active oxide groups exhibiting negative partials and high electronegativity. Consequently, the modified adsorbent undergoes an enhancement in adsorption capacity and exhibits substantial interaction energy between the adsorbent and adsorbate, preventing easy desorption [25].

From the R^2 shown in **Table 3**, both Langmuir and Freundlich isotherms in this study approach one, indicating that the observed adsorption is not limited to chemical interactions; physical adsorption is also evident. As also mentioned by Ragadhita and Nandiyanto [25], the Langmuir adsorption isotherm pertains to the adsorption process that occurs chemically, forming a monolayer on the adsorbent surface. In contrast, the Freundlich isotherm is employed to ascertain the physical adsorption process occurring on the heterogeneous active groups present on the surface of the adsorbent.

Following the identification of physisorption, it was also ascertained that $n > 1$, specifically 1.99 for the modified adsorbent and 1.78 for the unmodified adsorbent. A higher n value signifies increased heterogeneity in the adsorption process. This physical adsorption is primarily influenced by the adsorbent's magnetic field, enabling the adsorbent's porous surface, which lacks active groups, to interact with Pb^{2+} through Van Der Waals forces. Theoretically, this force is affected by the magnetic field on the adsorbent, which can reduce the solvent's (water) surface tension, thereby enhancing the mobility of the adsorbate. This results in the adsorbate being more effectively distributed across the adsorbent surface, leading to an

increase in material transfer between the adsorbent and adsorbate [26].

The parameters utilized to ascertain the adsorption capacity in the Freundlich isotherm are determined based on the K_f. A higher K_f corresponds to greater adsorption capacity; conversely, a lower K_f results in diminished adsorption capacity. The exact adsorption capacity on the Freundlich isotherm remains indeterminate as it depends on the initial concentration of the adsorbate.

Adsorption kinetics

Adsorption kinetics are established based on linear equations of the first, second, pseudo-first, and pseudo-second-order. Adsorption kinetics are related to the rate of adsorbate uptake by the adsorbent as expressed by the concentration versus time function. The first-order graph is generated using Eq. (5), plotting $\ln\frac{C_e}{C_0}$ versus time (t), while the second-order graph is constructed through Eq. (6) by plotting $\frac{1}{C_e}$ versus time t. The pseudo-first-order graph is determined according to Eq. (7) by plotting log(qe - qt) versus t, and the pseudo-second-order graph is created based on Eq. (8), representing the relationship between $\frac{t}{q_t}$ versus t.

$$\ln\frac{C_e}{C_0} = -k_1 t \quad (5)$$

$$\frac{1}{C_e} = k_2 t + \frac{1}{C_0} \quad (6)$$

$$\log(q_e - q_t) = \log q_e - \frac{k_3}{2{,}303} t \quad (7)$$

$$\frac{t}{q_t} = \frac{t}{q_e} + \frac{1}{k_4 q_e^2} \quad (8)$$

Adsorption kinetics are associated with the rate at which the adsorbent absorbs the adsorbate, expressed as a function of concentration over time. The suitable adsorption kinetics for the adsorption process, using both M-RM and U-RM adsorbents, is identified to be pseudo-second-order, as it exhibits a greater R^2 compared to those in the first-order, second-order, and pseudo-first-order graphs. The adsorption kinetics graph is shown in **Figures 4** and **5**, while the R^2 for each reaction order is presented in **Table 4**.

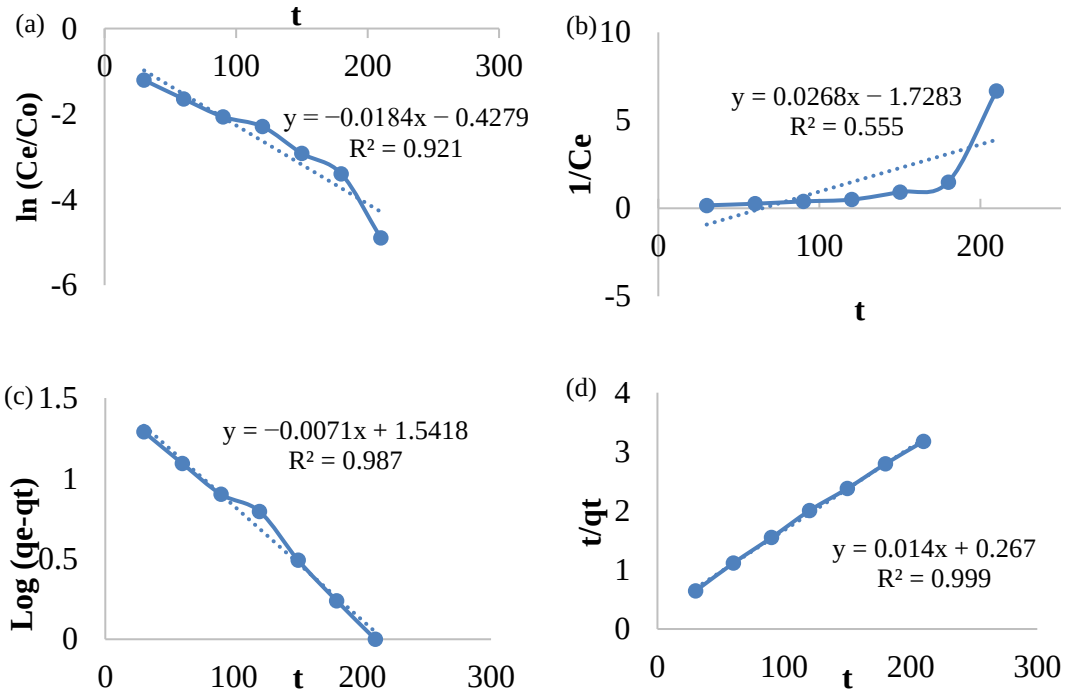

Figure 4 Adsorption kinetics of modified red mud: (a) first order, (b) second order, (c) pseudo-first order, and (d) pseudo-second order.

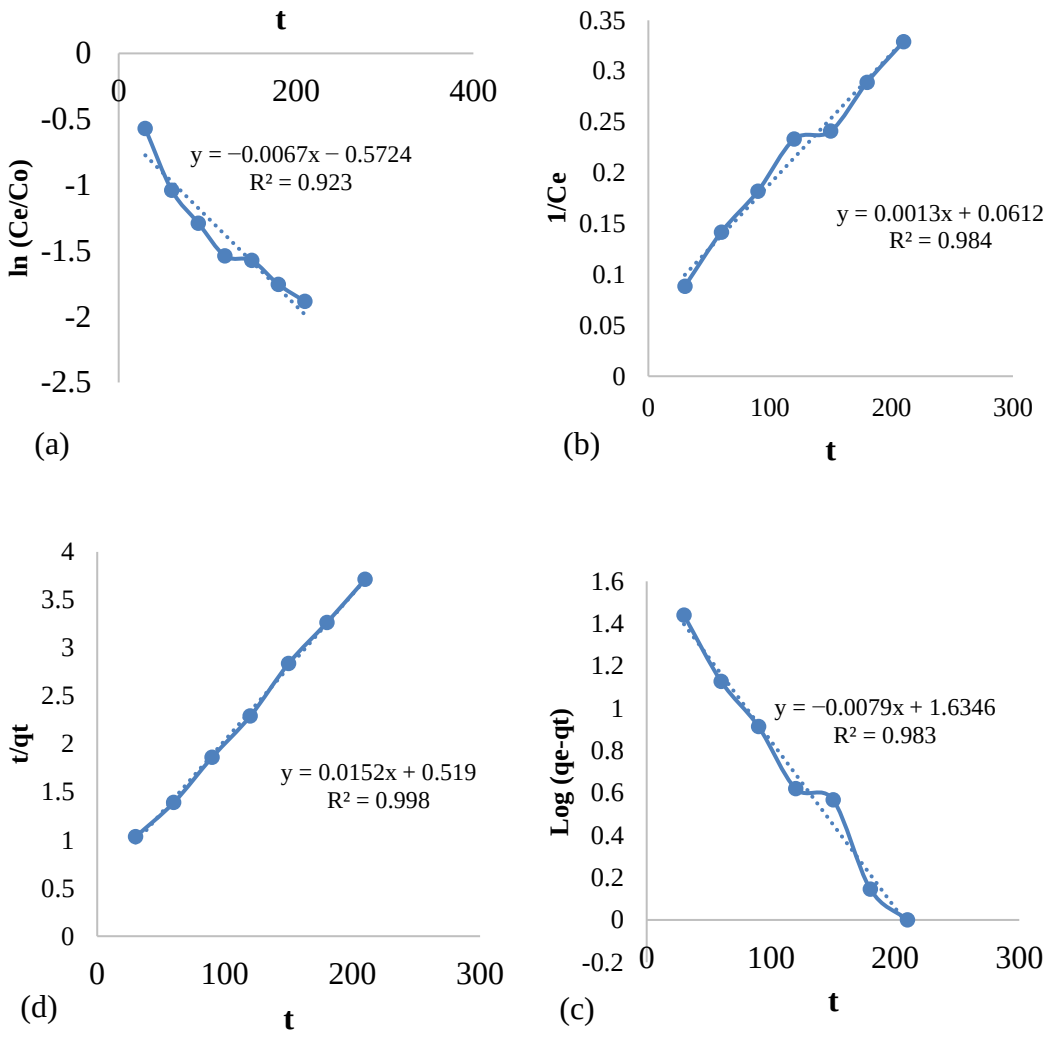

Figure 5 Adsorption kinetics of unmodified red mud: (a) first order, (b) second order, (c) pseudo-first order, and (d) pseudo-second order.

The pseudo-second-order adsorption kinetics indicates compatibility between the kinetics and adsorption isotherm, where each group on the adsorbent binds to one adsorbate ion, which can only occur in monolayer adsorption. The pseudo-second-order kinetics of the adsorbent is also evident in the initial reduction rate of the adsorbate concentration. The initial concentration of Pb(II), initially at 20 ppm, experiences a significant decrease at the beginning of adsorption using modified red mud and unmodified red mud adsorbents, reducing to 0.716 ppm and 11.3 ppm, respectively. The rate of adsorbate concentration reduction then gradually decreases until equilibrium conditions are reached.

Table 4 Adsorption Kinetics of modified and unmodified adsorbent.

Adsorbent	First order		Second order		Pseudo-first-order		Pseudo-second-order	
	R^2	k_1	R^2	k_2	R^2	k_3	R^2	k_4
M-RM	0.921	0.0184	0.555	0.0268	0.987	0.0164	0.999	7.4×10^{-4}
U-RM	0.923	0.0067	0.984	0.0013	0.983	0.0182	0.998	4.5×10^{-4}

The adsorption kinetic was studied by fitting the experimental data of pseudo-first-order (Eq. (9)) and pseudo-second-order (Eq. (10)). The pseudo-second-order model indicates that the adsorption rate of Pb(II) adsorbate on both M-RM and U-RM per unit time is directly proportional to the square of the remaining adsorption capacity of the adsorbent, which is not yet fully occupied by the adsorbate ($qe - qt$), as per Eq. (8). This suggests a stoichiometric 1:1 relationship between the adsorbent and the adsorbate, wherein one active group of the adsorbent will bind to one divalent metal ion (Pb^{2+}).

$$q_t = q_e(1 - e^{(-k_1 t)}) \quad (9)$$

$$q_t = \frac{k_2 q_e^2 t}{1 + k_2 q_e t} \quad (10)$$

where: q_t ($mg.g^{-1}$) represents the adsorption capacity of the adsorbent at time t; q_e ($mg.g^{-1}$) represents the equilibrium adsorption capacity; k_1 (min^{-1}) represents the adsorption rate constant of the pseudo-first-order kinetics model; k_2 ($g \cdot mg^{-1} \cdot min^{-1}$) represents the adsorption rate constant of the pseudo-second-order kinetics model.

Table 4 presents the pseudo-second-order reaction constant (k_4) for both adsorbents: 7.34×10^{-4} $ppm^{-1}min^{-1}$ for the M-RM adsorbent and 4.34×10^{-4} $ppm^{-1}min^{-1}$for the U-RM variant. The higher adsorption rate constant observed when using modified red mud adsorbent suggests it facilitates reaching adsorption equilibrium more promptly than its unmodified counterpart. Theoretically, the formation of magnetic minerals such as cancrinite, magnetite, and morimotoite in modified adsorbents imparts magnetic properties to the active groups in the adsorbent. Consequently, these magnetic properties render the active groups on the adsorbent, primarily FeO^-, negatively charged and endow them with high electronegativity, making them more amenable to interaction with the positively charged adsorbate, Pb^{2+}.

The observed pseudo-second-order adsorption kinetics aligns with the adsorption isotherm, indicating that each group on the adsorbent binds to a singular adsorbate ion, a phenomenon characteristic of monolayer adsorption. This pseudo-second-order nature is further evident in the rate at which the initial concentration of the adsorbate reduces. For instance, the initial concentration of Pb(II), initially set at 20 ppm, experienced a significant drop at the onset of adsorption with both M-RM and U-RM adsorbents, falling to 0.716 and 11.3 ppm, respectively. Subsequently, the rate of decrease in adsorbate concentration diminishes gradually until equilibrium is attained.

Conclusions

Several conclusions can be drawn from the undertaken study. Treating red mud with ascorbic acid initiates the reduction of various minerals, namely andradite, muscovite, and hematite, resulting in their transformation into cancrinite, morimotoite, and magnetite, respectively. This transformation leads to an enhancement in pore diameter, pore volume, and specific surface area of the adsorbent. Upon evaluating the adsorption isotherm model for Pb(II) metal ions using both modified and unmodified red mud adsorbents, it was established that the subsequent adsorption is consistent with both Langmuir and Freundlich isotherms, as evidenced by R^2 values nearing one. Concurrently, the adsorption kinetics exhibited by both adsorbent variants align with pseudo-second-order kinetics. Further, modifying red mud utilizing ascorbic acid amplifies the adsorbent's efficacy in adsorbing Pb(II) ions. It has been ascertained that such modification escalates the adsorption effectiveness to 99.3 %, compared to the 84.8 % effectiveness demonstrated by the unmodified red mud adsorbent.

Acknowledgements

The authors express our profound gratitude to Indonesia's Endowment Fund for Education for their invaluable support in making this research possible through the generous funding under the Program Riset Mandiri Dosen in Riset Keilmuan LPDP Kemendikbud Ristek 2021 - 2022.

References

[1] X Wang, T Sun, S Wu, C Chen, J Kou and C Xu. A novel utilization of Bayer red mud through co-reduction with a limonitic laterite ore to prepare ferronickel. *J. Clean. Prod.* 2019; **216**, 33-41.

[2] PJ Joyce, T Hertel, A Goronovski, AH Tkaczyk, Y Pontikes and A Björklund. Identifying hotspots of environmental impact in the development of novel inorganic polymer paving blocks from bauxite residue. *Resour. Conservat. Recycl.* 2018; **138**, 87-98.

[3] A Wahyudi, W Kurniawan, H Azhari, M Azis and H Hinode. Potential application of red mud (*Bauxite Residue*) in Indonesia. *In*: Proceedings of the Seminar-Workshop on Utilization of Waste Materials, Manila, Philippines, 2015. p. 57-62.
[4] MSS Lima, LP Thives, V Haritonovs and K Bajars. Red mud application in construction industry: Review of benefits and possibilities. *IOP Conf. Ser. Mater. Sci. Eng.* 2017; **251**, 012033.
[5] R Singh and R Bhateria. Optimization and experimental design of the Pb^{2+} adsorption process on a nano-Fe_3O_4-based adsorbent using the response surface methodology. *ACS Omega* 2020; **5**, 28305-18.
[6] Y Xu, Y Qu, Y Yang, B Qu, R Shan, H Yuan and Yong Sun. Study on efficient adsorption mechanism of Pb^{2+} by magnetic coconut biochar. *Int. J. Mol. Sci*. 2022; **23**, 14053.
[7] A Piekut, K Gut, M Cwielag-Drabek, J Domagalska and E Marchwinska-Wyrwał. The relationship between children's non-nutrient exposure to cadmium, lead and zinc and the location of recreational areas - based on the Upper Silesia region case (Poland). *Chemosphere* 2019; **223**, 544-50.
[8] A Setiawan, AN Rahmadania and NE Mayangsari. Adsorpsi Cu(II) menggunakan zeolit sintesis kombinasi abu terbang dan abu dasar dengan variasi waktu aging. *Jurnal Riset Teknologi Industri* 2021; **15**, 113.
[9] MK Sahu. 2017, Studies on the utilization of red mud for environmental application. Ph. D. Dissertation. National Institute of Technology, Rourkela, India.
[10] C Tsamo, PND, JMD Dikdim and R Kamga. Kinetic and equilibrium studies of Cr(VI), Cu(II) and Pb(II) removal from aqueous solution using red mud, a low-cost adsorbent. *Arab. J. Sci. Eng.* 2018; **43**, 2353-68.
[11] AN Babu, GVK Mohan, K Kalpana and K Ravindhranath. removal of lead from water using calcium alginate beads doped with hydrazine sulphate-activated red mud as adsorbent. *J. Anal. Meth. Chem.* 2017; **2017**, 4650594.
[12] W Dong, K Liang, Y Qin, H Ma, X Zhao, L Zhang, S Zhu, Y Yu, D Bian and J Yang. Hydrothermal conversion of red mud into magnetic adsorbent for effective adsorption of Zn(II) in water. *Appl. Sci.* 2019; **9**, 1519.
[13] YA Reddy, DK Babu, G Sreelatha and K Ravindhranath. Ascorbic acid tread red mud immobilized in ca-alginate beads as an effective adsorbent for the removal of copper ions from industrial wastewater. *Rasayan J. Chem.* 2021; **14**, 397-408.
[14] Y Li, H Huang, Z Xu, H Ma and Y Guo. Mechanism study on manganese(II) removal from acid mine wastewater using red mud and its application to a lab-scale column. *J. Clean. Prod*. 2020; **253**, 119955.
[15] NV Chukanov and AD Chervonnyi. *Infrared spectroscopy of minerals and related compounds*. Springer, Cham, Switzerland, 2016.
[16] NV Chukanov and MF Vigasina. *Vibrational (infrared and raman) spectra of minerals and related compounds*. Springer, Cham, Switzerland, 2020.
[17] E Bertolucci, AMR Galletti, C Antonetti, M Marracci, B Tellini, F Piccinelli and C Visone. Chemical and magnetic properties characterization of magnetic nanoparticles. *In*: Proceedings of the 2015 IEEE International Instrumentation and Measurement Technology Conference (I2MTC) Proceedings, Pisa, Italy, 2015. p.1492-6
[18] XN Pham, TP Nguyen, TN Pham, TTN Tran and TVT Tran. Synthesis and characterization of chitosan-coated magnetite nanoparticles and their application in curcumin drug delivery. *Adv. Nat. Sci. Nanosci. Nanotech.* 2016; **7**, 045010.
[19] CC Huang. Microstructure and thermal property of designed alginate-based polymeric composite foam materials containing biomimetic decellularized elastic cartilage microscaffolds. *Materials* 2022; **15**, 258.
[20] BC Smith. Alcohols - the rest of the story. *Spectroscopy* 2017; **32**, 19-23.
[21] O Kazak and A Tor. In situ preparation of magnetic hydrochar by co-hydrothermal treatment of waste vinasse with red mud and its adsorption property for Pb(II) in aqueous solution. *J. Hazard. Mater.* 2020; **393**, 122391.
[22] I Nurhidayati, B Mellisani, F Puspita and RAF Putri. Penentuan isoterm dan kinetika asorpsi ion besi oleh sedimen sebagai adsorben. *Warta Akab* 2022; **46**, 75-83.
[23] J Shi, H Zhang, Y Yu, X Zou, W Zhou, J Guo, Y Ye and Y Zhao. Adsorption properties of calcium alginate-silica dioxide hybrid adsorbent to methylene blue. *J. Inorg. Organomet. Polymer. Mater.* 2020; **30**, 2114-25.

[24] A Mohammed, R Bissoon, E Bajnath, K Mohammed, T Lee, M Bissram, N John, NK Jalsa, KY Lee and K Ward. Multistage extraction and purification of waste Sargassum natans to produce sodium alginate: An optimization approach. *Carbohydr. Polymer.* 2018; **198**, 109-18.
[25] R Ragadhita and ABD Nandiyanto. How to calculate adsorption isotherms of particles using two-parameter monolayer adsorption models and equations. *Indonesian J. Sci. Tech.* 2021; **6**, 205-34.
[26] A Fillaeli, ED Siswani, S Kristianingrum, S Sulistyani and AD Pratiwi. Adsorpsi multilogam untuk penurunan kadar Cu, Fe, Ni dan Zn menggunakan arang aktif daun pandan laut. *Jurnal Sains Dasar* 2019; **8**, 64-9.